

# Architectural Complexity Measures of Recurrent Neural Networks

Saizheng Zhang<sup>1,\*</sup>

Yuhuai Wu<sup>2,\*</sup>

Tong Che<sup>3</sup>

Zhouhan Lin<sup>1</sup>

Roland Memisevic<sup>1,5</sup>

Ruslan Salakhutdinov<sup>4,5</sup>

Yoshua Bengio<sup>1,5</sup>

<sup>1</sup>Université de Montréal, <sup>2</sup>University of Toronto, <sup>3</sup>Institut des Hautes Études Scientifiques, France, <sup>4</sup>Carnegie-Mellon University, <sup>5</sup>CIFAR

\* Equal contribution

SAIZHENG.ZHANG@UMONTREAL.CA

YWU@CS.TORONTO.EDU

TONGCHE@IHES.FR

LIN.ZHOUHAN@GMAIL.COM

ROLAND.UMONTREAL@GMAIL.COM

RSALAKHU@CS.TORONTO.EDU

YOSHUA.BENGIO@GMAIL.COM

## Abstract

In this paper, we systematically analyse the connecting architectures of recurrent neural networks (RNNs). Our main contribution is twofold: first, we present a rigorous graph-theoretic framework describing the connecting architectures of RNNs in general. Second, we propose three architecture complexity measures of RNNs: (a) the **recurrent depth**, which captures the RNN’s over-time nonlinear complexity, (b) the **feedforward depth**, which captures the local input-output nonlinearity (similar to the “depth” in feedforward neural networks (FNNs)), and (c) the **recurrent skip coefficient** which captures how rapidly the information propagates over time. Our experimental results show that RNNs might benefit from larger recurrent depth and feedforward depth. We further demonstrate that increasing recurrent skip coefficient offers performance boosts on long term dependency problems, as we improve the state-of-the-art for sequential MNIST dataset.

## 1. Introduction

Recurrent neural networks (RNNs) have been shown to achieve promising results on many difficult sequential learning problems (Graves, 2013; Bahdanau et al., 2014; Sutskever et al., 2014; Srivastava et al., 2015; Kiros et al., 2015). There is also much work attempting to reveal the principles behind the challenges and successes of RNNs, including optimization issues (Martens & Sutskever, 2011; Pascanu et al., 2013b), gradient vanishing/exploding related problems (Hochreiter, 1991; Bengio et al., 1994), analysing/designing new RNN transition functional units

like LSTMs, GRUs and their variants (Hochreiter & Schmidhuber, 1997; Greff et al., 2015; Cho et al., 2014; Jozefowicz et al., 2015).

This paper focuses on another important theoretical aspect of RNNs: the connecting architecture. Ever since Schmidhuber (1992); El Hihi & Bengio (1996) introduced different forms of “stacked RNNs”, researchers have taken architecture design for granted and have paid less attention to the exploration of other connecting architectures. Some examples include Raiko et al. (2012); Graves (2013) who explored the use of skip connections; Hermans & Schrauwen (2013) who proposed the deep RNNs which are stacked RNNs with skip connections; Pascanu et al. (2013a) who pointed out the distinction of constructing a “deep” RNN from the view of the recurrent paths and the view of the input-to-hidden and hidden-to-output maps. However, they did not rigorously formalize the notion of “depth” and its implications in “deep” RNNs. Besides “deep” RNNs, there still remains a vastly unexplored field of connecting architectures. We argue that one barrier for better understanding the architectural complexity is the lack of a general definition of the connecting architecture. This forced previous researchers to mostly consider the simple cases while neglecting other possible connecting variations. Another barrier is the lack of quantitative measurements of the complexity of different RNN connecting architectures: even the concept of “depth” is not clear with current RNNs.

In this paper, we try to address these two barriers. We first introduce a general definition of a recurrent neural network, where we divide an RNN into two basic ingredients: a well-defined graph representation of the connecting architecture, and a set of transition functions describing the computational process associated with each unit in the network. Observing that the RNN undergoes multiple transformations not only feedforwardly (from input to output within a

time step) but also recurrently (across multiple time steps), we carry out a quantitative analysis of the number of transformations in these two orthogonal directions, which results in the definitions of *recurrent depth* and *feedforward depth*. These two depths can be viewed as general extensions of the work of Pascanu et al. (2013a). We also explore a quantity called the *recurrent skip coefficient* which measures how quickly information propagates over time. This quantity is strongly related to vanishing/exploding gradient issues, and helps deal with long term dependency problems. Skip connections crossing different timescales have also been studied by Lin et al. (1996); El Hiji & Bengio (1996); Sutskever & Hinton (2010); Koutnik et al. (2014). Instead of specific architecture design, we focus on analyzing the graph-theoretic properties of recurrent skip coefficients, revealing the fundamental difference between the regular skip connections and the ones which truly increase the recurrent skip coefficients.

We empirically evaluate models with different recurrent/feedforward depths and recurrent skip coefficients on language modelling and sequential MNIST tasks. We also show that our experimental results further validate the usefulness of the proposed definitions.

## 2. General RNN

RNNs are learning machines that recursively compute new states by applying transition functions to previous states and inputs. It has two ingredients: the connecting architecture describing how information flows between different nodes and the transition function describing the nonlinear transformation at each node. The connecting architecture is usually illustrated informally by an infinite directed acyclic graph, which in turn can be viewed as a finite directed cyclic graph that is unfolded through time. In this section, we first introduce a general definition of the connecting architecture and its underlying computation, followed by a general definition of an RNN.

### 2.1. The Connecting Architecture

We formalize the concept of the connecting architecture by extending the traditional graph-based illustration to a more general definition with a *finite directed multigraph* and its *unfolded* version. Let us first define the notion of the *RNN cyclic graph*  $\mathcal{G}_c$  that can be viewed as a cyclic graphical representation of RNNs. We attach “weights” to the edges in the cyclic graph  $\mathcal{G}_c$  that represent time delay differences between the source and destination node in the unfolded graph representation.

**Definition 2.1.1.** Let  $\mathcal{G}_c = (V_c, E_c)$  be a weighted directed multigraph<sup>1</sup>, in which  $V_c = V_{in} \cup V_{out} \cup V_{hid}$  is a finite set

<sup>1</sup>A directed multigraph is a directed graph that allows multiple

of nodes, and  $V_{in}, V_{out}, V_{hid}$  are not empty.  $E_c \subset V_c \times V_c \times \mathbb{Z}$  is a finite set of directed edges. Each  $e = (u, v, \sigma) \in E_c$  denotes a directed weighted edge pointing from node  $u$  to node  $v$  with an integer weight  $\sigma$ . Each node  $v \in V_c$  is labelled by an integer tuple  $(i, p)$ .  $i \in \{0, 2, \dots, m-1\}$  denotes the time index of the given node, where  $m$  is the **period number** of the RNN, and  $p \in S$ , where  $S$  is a finite set of node labels. We call the weighted directed multigraph  $\mathcal{G}_c = (V_c, E_c)$  an RNN cyclic graph, if

(1) For every edge  $e = (u, v, \sigma) \in E_c$ , let  $i_u$  and  $i_v$  denote the time index of node  $u$  and  $v$ , then  $\sigma = i_v - i_u + k \cdot m$  for some  $k \in \mathbb{Z}$ .

(2) There exists at least one directed cycle<sup>2</sup> in  $\mathcal{G}_c$ .

(3) For any closed walk  $\omega$ , the sum of all the  $\sigma$  along  $\omega$  is not zero.

(4) There are no incoming edges to nodes in  $V_{in}$ , and no outgoing edges from nodes in  $V_{out}$ . There are both incoming edges and outgoing edges for nodes in  $V_{hid}$ .

Condition (1) assures that we can get a periodic graph (repeating pattern) when unfolding the RNN through time. Condition (2) excludes feedforward neural networks in the definition by forcing to have at least one cycle in the cyclic graph. Condition (3) simply avoids cycles after unfolding.

The cyclic representation can be seen as a time folded representation of RNNs, as shown in Figure 1 (a). Given an RNN cyclic graph  $\mathcal{G}_c$ , we unfold  $\mathcal{G}_c$  over time  $t \in \mathbb{Z}$  by the following procedure:

**Definition 2.1.2 (Unfolding).** Given an RNN cyclic graph  $\mathcal{G}_c = (V_c, E_c, \sigma)$ , we define a new infinite set of nodes  $V_{un} = \{(i + km, p) | (i, p) \in V, k \in \mathbb{Z}\}$ . The new set of edges  $E_{un} \subset V_{un} \times V_{un}$  is constructed as follows:  $((t, p), (t', p')) \in E_{un}$  if and only if there is an edge  $e = ((i, p), (i', p'), \sigma) \in E$  such that  $t' - t = \sigma$ , and  $t \equiv i \pmod{m}$ . The new directed graph  $\mathcal{G}_{un} = (V_{un}, E_{un})$  is called the unfolding of  $\mathcal{G}_c$ . Any infinite directed graph that can be constructed from an RNN cyclic graph through unfolding is called an RNN unfolded graph.

**Lemma 2.1.1.** The unfolding  $\mathcal{G}_{un}$  of any RNN cyclic graph  $\mathcal{G}_c$  is a directed acyclic graph (DAG).

Figure 1(a) shows an example of two graph representations  $\mathcal{G}_{un}$  and  $\mathcal{G}_c$  of a given RNN. Consider the edge from node  $(1, 7)$  going to node  $(0, 3)$  in  $\mathcal{G}_c$ . The fact that it has weight 1 indicates that the corresponding edge in  $\mathcal{G}_{un}$  travels one time step,  $((t+1, 7), (t+2, 3))$ . Note that node  $(0, 3)$  also has a loop with weight 2. This loop corresponds to the edge  $((t, 3), (t+2, 3))$ .

The two kinds of graph representations we presented above directed edges connecting two nodes.

<sup>2</sup>A directed cycle is a closed walk with no repetitions of edges.

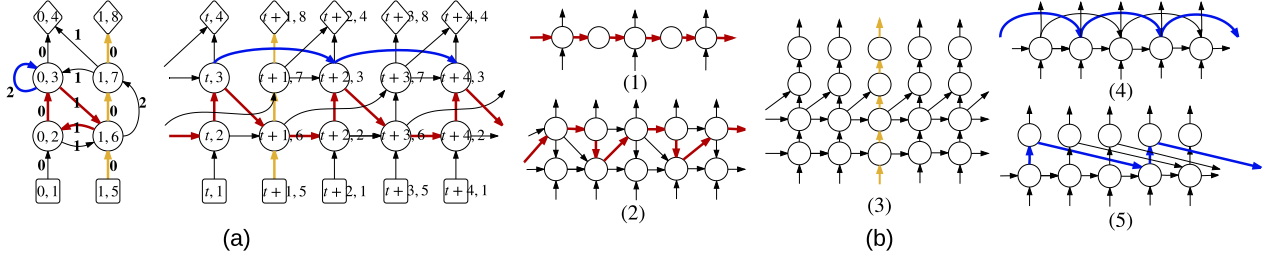


Figure 1. (a) An example of an RNN’s  $\mathcal{G}_c$  and  $\mathcal{G}_{un}$ .  $V_{in}$  is denoted by square,  $V_{hid}$  is denoted by circle and  $V_{out}$  is denoted by diamond. In  $\mathcal{G}_c$ , the number on each edge is its corresponding  $\sigma$ . The longest path is colored in red. The longest input-output path is colored in yellow and the shortest path is colored blue. The value of three measures are  $d_r = \frac{3}{2}$ ,  $d_f = 3$  and  $s = 2$ . (b) 5 more examples. (1) and (2) have  $d_r = 2, \frac{3}{2}$ , (3) has  $d_f = 5$ , (4) and (5) has  $s = 2, \frac{3}{2}$ .

have a one-to-one correspondence. Also, any graph structure  $\theta$  on  $\mathcal{G}_{un}$  is naturally mapped into a graph structure  $\bar{\theta}$  on  $\mathcal{G}_c$ . Given an edge tuple  $\bar{e} = (u, v, \sigma)$  in  $\mathcal{G}_c$ ,  $\sigma$  stands for the number of time steps crossed by  $\bar{e}$ ’s covering edges in  $E_{un}$ , i.e., for every corresponding edge  $e \in \mathcal{G}_{un}$ ,  $e$  must start from some time index  $t$  to  $t + \sigma$ . Hence  $\sigma$  corresponds to the “time delay” associated with  $e$ .

In addition, the *period number*  $m$  in Definition 2.1.1 can be interpreted as the time length of the entire non-repeated recurrent structure in its unfolded RNN graph  $\mathcal{G}_{un}$ . Strictly speaking,  $m$  has the following properties in  $\mathcal{G}_{un}$ :  $\forall k \in \mathbb{Z}$ , if  $\exists v = (t, p) \in V_{un}$ , then  $\exists v' = (t + km, p) \in V_{un}$ ; if  $\exists e = ((t, p), (t', p')) \in E_{un}$ , then  $\exists e' = ((t + km, p), (t' + km, p')) \in E_{un}$ . In other words, shifting the  $\mathcal{G}_{un}$  through time by  $km$  time steps will result in a DAG which is identical to  $\mathcal{G}_{un}$ , and  $m$  is the smallest number that has such property for  $\mathcal{G}_{un}$ . Most traditional RNNs have  $m = 1$ , while some special structures like *hierarchical* or *clock-work RNN* (El Hihi & Bengio, 1996; Koutnik et al., 2014) have  $m > 1$ . For example, Figure 1(a) (unfolded graph representation  $\mathcal{G}_{un}$ ) shows that the period number of this specific RNN is 2.

It is clear that if there exists a directed cycle  $\vartheta$  in  $\mathcal{G}_c$ , and the sum of  $\sigma$  along  $\vartheta$  is positive (or negative), then there is a path which is the pre-image of  $\vartheta$  in  $\mathcal{G}_{un}$  whose length (summing the edge  $\sigma$ ’s) approaches  $+\infty$  (or  $-\infty$ ). This fact naturally induces the general definition of unidirectionality and bidirectionality of RNNs as follows:

**Definition 2.1.3.** An RNN is called *unidirectional* if its cyclic graph representation  $\mathcal{G}_c$  has the property that the sums of  $\sigma$  along all the directed cycles  $\vartheta$  in  $\mathcal{G}_c$  share the same sign, i.e., either all positive or all negative. An RNN is called *bidirectional* if it is not unidirectional.

## 2.2. A General Definition of RNN

The connecting architecture in Sec. 2.1 describes how information flows among RNN units. Assume  $\bar{v} \in V_c$  is a node in  $\mathcal{G}_c$ , let  $\text{In}(\bar{v})$  denotes the set of incoming nodes of  $\bar{v}$ ,  $\text{In}(\bar{v}) = \{\bar{u} | (\bar{u}, \bar{v}) \in E_c\}$ . In the forward pass of the RNN, the transition function  $F_{\bar{v}}$  takes outputs of nodes  $\text{In}(\bar{v})$  as

inputs and computes a new output. For example, vanilla RNNs units with different activation functions, LSTMs and GRUs can all be viewed as units with specific transition functions.

We now give the general definition of an RNN:

**Definition 2.2.1.** An RNN is a tuple  $(\mathcal{G}_c, \mathcal{G}_{un}, \{F_{\bar{v}}\}_{\bar{v} \in V_c})$ , in which  $\mathcal{G}_{un} = (V_{un}, E_{un})$  is the unfolding of RNN cyclic graph  $\mathcal{G}_c$ , and  $\{F_{\bar{v}}\}_{\bar{v} \in V_c}$  is the set of transition functions. In the forward pass, for each hidden and output node  $v \in V_{un}$ , the transition function  $F_{\bar{v}}$  takes all incoming nodes of  $v$  as the input to compute the output.

An RNN is *homogeneous* if all the hidden nodes share the same form of the transition function.

## 3. Measures of Architectural Complexity

In this section, we develop different measures of RNNs’ architectural complexity, focusing mostly on the graph-theoretic properties of RNNs. To analyze an RNN solely from its architectural aspect, we make the mild assumption that the RNN is homogeneous. We further assume the RNN to be unidirectional. For a bidirectional RNN, it is more natural to measure the complexities of its unidirectional components.

### 3.1. Recurrent Depth

Unlike feedforward models where computations are done within one time frame, RNNs map inputs to outputs over multiple time steps. In some sense, an RNN undergoes transformations along both feedforward and recurrent dimensions. This fact suggests that we should investigate its architectural complexity from these two different perspectives. We first consider the recurrent perspective.

The conventional definition of depth is the *maximum* number of nonlinear transformations from inputs to outputs. Observe that a directed path in an unfolded graph representation  $\mathcal{G}_{un}$  corresponds to a sequence of nonlinear transformations. Given an unfolded RNN graph  $\mathcal{G}_{un}$ ,  $\forall i, n \in \mathbb{Z}$ , let  $\mathcal{D}_i(n)$  be the length of the *longest* path from any node

at starting time  $i$  to any node at time  $i + n$ .

From the recurrent perspective, it is natural to investigate how  $\mathfrak{D}_i(n)$  changes over time. Generally speaking,  $\mathfrak{D}_i(n)$  increases as  $n$  increases for all  $i$ . Such increase is caused by the recurrent structure of the RNN which keeps adding new nonlinearities over time. Since  $\mathfrak{D}_i(n)$  approaches  $\infty$  as  $n$  approaches  $\infty$ ,<sup>3</sup> to measure the complexity of  $\mathfrak{D}_i(n)$ , we consider its asymptotic behaviour, i.e., the limit of  $\frac{\mathfrak{D}_i(n)}{n}$  as  $n \rightarrow \infty$ . Under a mild assumption, this limit exists. To perform a practical calculation of this limit, the next theorem relies on  $\mathcal{G}_{\text{un}}$ 's cyclic counterpart  $\mathcal{G}_c$ , where the computation is much easier:

**Theorem 3.2 (Recurrent Depth).** *Given an RNN and its two graph representation  $\mathcal{G}_{\text{un}}$  and  $\mathcal{G}_c$ , we denote  $C(\mathcal{G}_c)$  to be the set of directed cycles in  $\mathcal{G}_c$ . For  $\vartheta \in C(\mathcal{G}_c)$ , let  $l(\vartheta)$  denote the length of  $\vartheta$  and  $\sigma_s(\vartheta)$  denote the sum of edge weights  $\sigma$  along  $\vartheta$ . Under a mild assumption<sup>4</sup>,*

$$d_r = \lim_{n \rightarrow +\infty} \frac{\mathfrak{D}_i(n)}{n} = \max_{\vartheta \in C(\mathcal{G}_c)} \frac{l(\vartheta)}{\sigma_s(\vartheta)}. \quad (1)$$

Thus,  $d_r$  is a positive rational number.

More intuitively,  $d_r$  is a measure of the average maximum number of nonlinear transformations per time step as  $n$  gets large. Thus, we call it *recurrent depth*:

**Definition 3.2.1 (Recurrent Depth).** *Given an RNN and its two graph representations  $\mathcal{G}_{\text{un}}$  and  $\mathcal{G}_c$ , we call  $d_r$ , defined in Eq.(1), the recurrent depth of the RNN.*

In Figure 1(a), one can easily verify that  $\mathfrak{D}_i(1) = 5$ ,  $\mathfrak{D}_i(2) = 6$ ,  $\mathfrak{D}_i(3) = 8$ ,  $\mathfrak{D}_i(4) = 9 \dots$ . Thus  $\frac{\mathfrak{D}_i(1)}{1} = 5$ ,  $\frac{\mathfrak{D}_i(2)}{2} = 3$ ,  $\frac{\mathfrak{D}_i(3)}{3} = \frac{8}{3}$ ,  $\frac{\mathfrak{D}_i(4)}{4} = \frac{9}{4} \dots$ , which eventually converges to  $\frac{3}{2}$  as  $n \rightarrow \infty$ . As  $n$  increases, most parts of the longest path coincides with the path colored in red. As a result,  $d_r$  coincides with the number of nodes the red path goes through per time step. Similarly in  $\mathcal{G}_c$ , observe that the red cycle achieves the maximum ( $\frac{3}{2}$ ) in Eq.(1). Usually, one can directly calculate  $d_r$  from  $\mathcal{G}_{\text{un}}$ .

It is easy to verify that *simple RNNs* and *stacked RNNs* share the same recurrent depth which is equal to 1. This reveals the fact that their nonlinearities increase at the same rate, which suggests that they will behave similarly in the long run. This fact is often neglected, since one would typically consider the number of layers as a measure of depth, and think of stacked RNNs as “deep” and simple RNNs as “shallow”, even though their discrepancies are not due to recurrent depth (which regards time) but due to feedforward depth, defined next.

<sup>3</sup>Without loss of generality, we assume the unidirectional RNN approaches positive infinity.

<sup>4</sup>See a full treatment of the limit in general cases in Theorem A.1 and Proposition A.1.1 in Appendix.

### 3.3. Feedforward Depth

Recurrent depth does not fully characterize the nature of nonlinearity of an RNN. As previous work suggests (Sutskever et al., 2014), stacked RNNs do outperform shallow ones with the same hidden size on problems where a more immediate input and output process is modeled. This is not surprising, since the growth rate of  $\mathfrak{D}_i(n)$  only captures the number of nonlinear transformations in the time direction, not in the feedforward direction.

The perspective of feedforward computation puts more emphasis on the specific paths connecting inputs to outputs. Given an RNN unfolded graph  $G_{\text{un}}$ , let  $\mathfrak{D}_i^*(n)$  be the length of the longest path from any input node at time step  $i$  to any output node at time step  $i + n$ . Clearly, when  $n$  is small, the recurrent depth cannot serve as a good description for  $\mathfrak{D}_i^*(n)$ . In fact, it heavily depends on another quantity which we call *feedforward depth*. The following proposition guarantees the existence of such a quantity and demonstrates the role of both measures in quantifying the nonlinearity of an RNN.

**Proposition 3.3.1 (Input-Output Length Least Upper Bound).** *Given an RNN with recurrent depth  $d_r$ , we denote*

$$d_f = \sup_{i, n \in \mathbb{Z}} \mathfrak{D}_i^*(n) - n \cdot d_r. \quad (2)$$

*The supremum  $d_f$  exists and thus we have the following upper bound for  $\mathfrak{D}_i^*(n)$*

$$\mathfrak{D}_i^*(n) \leq n \cdot d_r + d_f.$$

The above upper bound explicitly shows the interplay between recurrent depth and feedforward depth: when  $n$  is small,  $\mathfrak{D}_i^*(n)$  is largely bounded by  $d_f$ ; when  $n$  is large,  $d_r$  captures the nature of the bound ( $\approx n \cdot d_r$ ). These two measures are equally important, as they separately capture the maximum number of nonlinear transformations of an RNN in the long run and in the short run.

**Definition 3.3.1. (Feedforward Depth)** *Given an RNN with recurrent depth  $d_r$  and its two graph representations  $\mathcal{G}_{\text{un}}$  and  $\mathcal{G}_c$ , we call  $d_f$ , defined in Eq.(2), the feedforward depth<sup>5</sup> of the RNN.*

To calculate  $d_f$  in practice, we introduce the following theorem:

**Theorem 3.4 (Feedforward Depth).** *Given an RNN and its two graph representations  $\mathcal{G}_{\text{un}}$  and  $\mathcal{G}_c$ , we denote  $\xi(\mathcal{G}_c)$  the set of directed paths that start at an input node and end*

<sup>5</sup>Conventionally, an architecture with depth 1 is a three-layer architecture containing one hidden layer. But in our definition, since it goes through two transformations, we count the depth as 2 instead of 1. This should be particularly noted with the concept of feedforward depth, which can be thought as the conventional depth plus 1.



at an output node in  $\mathcal{G}_c$ . For  $\gamma \in \xi(\mathcal{G}_c)$ , denote  $l(\gamma)$  the length and  $\sigma_s(\gamma)$  the sum of  $\sigma$  along  $\gamma$ . Then we have:

$$d_f = \sup_{i, n \in \mathbb{Z}} \mathfrak{D}_i^*(n) - n \cdot d_r = \max_{\gamma \in \xi(\mathcal{G}_c)} l(\gamma) - \sigma_s(\gamma) \cdot d_r,$$

where  $m$  is the period number and  $d_r$  is the recurrent depth of the RNN. Thus,  $d_f$  is a positive rational number.

For example, in Figure 1(a), one can easily verify that  $d_f = \mathfrak{D}_t^*(0) = 3$ . Most commonly,  $d_f$  is the same as  $\mathfrak{D}_t^*(0)$ , i.e., the maximum length from an input to its current output.

### 3.5. Recurrent Skip Coefficient

Depth provides a measure of the complexity of the model. But such a measure is not sufficient to characterize behavior on long-term dependency tasks. In particular, since models with large recurrent depths have more nonlinearities through time, gradients can explode or vanish more easily. On the other hand, it is known that adding skip connections across multiple time steps may help improve the performance on long-term dependency problems (Lin et al. (1996); Sutskever & Hinton (2010)). To measure such a “skipping” effect, we should instead pay attention to the length of the *shortest path* from time  $i$  to time  $i + n$ . In  $\mathcal{G}_{un}$ ,  $\forall i, n \in \mathbb{Z}$ , let  $\mathfrak{d}_i(n)$  be the length of the shortest path. Similar to the recurrent depth, we consider the growth rate of  $\mathfrak{d}_i(n)$ .

**Theorem 3.6 (Recurrent Skip Coefficient).** *Given an RNN and its two graph representations  $\mathcal{G}_{un}$  and  $\mathcal{G}_c$ , under mild assumptions<sup>6</sup>*

$$j = \lim_{n \rightarrow +\infty} \frac{\mathfrak{d}_i(n)}{n} = \min_{\vartheta \in C(\mathcal{G}_c)} \frac{l(\vartheta)}{\sigma_s(\vartheta)}. \quad (3)$$

Thus,  $j$  is a positive rational number.

Since it is often the case that  $j$  is smaller or equal to 1, it is more intuitive to consider its reciprocal.

**Definition 3.6.1. (Recurrent Skip Coefficient)<sup>7</sup>.** *Given an RNN and its two graph representations  $\mathcal{G}_{un}$  and  $\mathcal{G}_c$ , we define  $s = \frac{1}{j}$ , whose reciprocal is defined in Eq.(3), as the recurrent skip coefficient of the RNN.*

With a larger recurrent skip coefficient, the number of transformations per time step is smaller. As a result, the nodes in the RNN are more capable of “skipping” across the network, allowing unimpeded information flow across multiple time steps, thus alleviating the problem of learning long term dependencies. In particular, such effect is more prominent in the long run, due to the network’s recurrent

structure. Also note that not all types of skip connections can increase the recurrent skip coefficient. We will consider specific examples in our experimental results section.

## 4. Experiments and Results

In this section we conduct a series of experiments to investigate the following questions: (1) Is recurrent depth a trivial measure? (2) Can increasing depth yield performance improvements? (3) Can increasing the recurrent skip coefficient improve the performance on long term dependency tasks? (4) Does the recurrent skip coefficient suggest something more compared to simply adding skip connections? We first show evaluations on RNNs with *tanh* nonlinearities, and then present similar results for LSTMs.

### 4.1. Tasks and Training Settings

**text8 dataset:** We evaluate our models on character level language modeling using the text8 dataset<sup>8</sup>, which contains 100M characters from Wikipedia with an alphabet of letters *a-z* and a space symbol. We follow the setting from Mikolov et al. (2012): 90M for training, 5M for validation and the remaining 5M for test. We also divide the training set into non-overlapping sequences, each of length 180. Quality of fit is evaluated by the bits-per-character (BPC) metric, which is  $\log_2$  of perplexity.

**sequential MNIST dataset:** We also evaluate our models with a modified version of the MNIST dataset. Each MNIST image data is reshaped into a  $784 \times 1$  sequence, turning the digit classification task into a sequence classification one with long-term dependencies (Le et al., 2015; Arjovsky et al., 2015). The model has access to 1 pixel per time step and predicts the class label at the end. A slight modification of the dataset is to permute the image sequences by a fixed random order beforehand (permuted MNIST). Since spatially local dependencies are no longer local (in the sequence), this task may be harder in terms of modelling long-term dependencies. Results in Le et al. (2015) have shown that both *tanh* RNNs and LSTMs did not achieve satisfying performance, which also highlights the difficulty of this task.

For all of our experiments we use *Adam* (Kingma & Ba, 2014) for optimization, and conduct a grid search on the learning rate in  $\{10^{-2}, 10^{-3}, 10^{-4}, 10^{-5}\}$ . For *tanh* RNNs, the parameters are initialized with samples from a uniform distribution. For LSTM networks we adopt a similar initialization scheme, while the forget gate biases are chosen by the grid search on  $\{-5, -3, -1, 0, 1, 3, 5\}$ . We employ early stopping and the batch size was set to 50.

<sup>6</sup>See Proposition A.3.1 in Appendix.

<sup>7</sup>One would find this definition very similar to the definition of the recurrent depth. Therefore, we refer readers to examples in Figure 1 for some illustrations.

<sup>8</sup><http://mattmahoney.net/dc/textdata>.

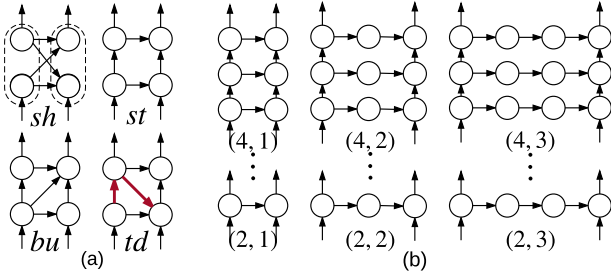


Figure 2. (a) the architectures for *sh*, *st*, *bu* and *td*, with their  $(d_r, d_f)$  equal to  $(1, 2)$ ,  $(1, 3)$ ,  $(1, 3)$  and  $(2, 3)$ , respectively. The longest path in *td* are colored in red. (b) The 9 architectures denoted by their  $(d_f, d_r)$  with  $d_r = 1, 2, 3$  and  $d_f = 2, 3, 4$ . We only plot the hidden states within 1 time step (which also have a period of 1) in both (a) and (b).

#### 4.2. Recurrent Depth is Non-trivial

To investigate the first question, we compare 4 similar connecting architectures: 1-layer (shallow) “*sh*”, 2-layers stacked “*st*”, 2-layers stacked with an extra bottom-up connection “*bu*”, and 2-layers stacked with an extra top-down connection “*td*”, as shown in Figure 2(a). *sh* has a layer size of 512, while the rest of the networks have a layer size of 256, making the number of hidden parameters in each architecture remain roughly the same. We also compare our results to the ones reported in Pascanu et al. (2012) (denoted as “P-*sh*”), since they used the same model architecture as the one specified by our *sh*.

Although the four architectures look quite similar, they have different recurrent depths: *sh*, *st* and *bu* have  $d_r = 1$ , while *td* has  $d_r = 2$ . Note that the specific construction of the extra nonlinear transformations in *td* is not conventional. Instead of simply adding intermediate layers in hidden-to-hidden connection, as reported in Pascanu et al. (2013a), more nonlinearities are gained by a recurrent flow from the first layer to the second layer and then back to the first layer at each time step (see the red path in Figure 2(a)).

Table 1. test BPCs of <i>sh</i> , <i>st</i> , <i>bu</i> , <i>td</i> for <i>tanh</i> RNNs					
TEST BPC	<i>sh</i>	<i>st</i>	<i>bu</i>	<i>td</i>	P- <i>sh</i>
<i>text8</i>	1.80	1.82	1.80	<b>1.77</b>	1.80

Table 1 clearly shows that the *td* architecture outperforms all the other architectures, including the one reported in Pascanu et al. (2012). The validation curve, displayed in Figure 3(a), further shows the gap between *td* and the other three architectures. Even though *td*’s validation BPC is higher at the beginning of the training (possibly due to harder initial optimization), it outperforms all other architectures in the long run.

It is also interesting to note the improvement we obtain when switching from *bu* to *td*. The only difference between these two architectures lies in changing the direction of one connection (see Figure 2(a)), which also increases

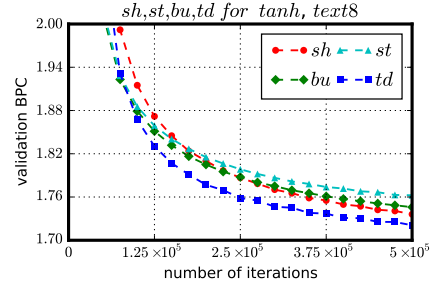


Figure 3. Validation curves of *sh*, *st*, *bu* and *td* on *text8* dataset.

the recurrent depth. Such a fundamental difference is by no means self-evident, but this result highlights the necessity of the concept of recurrent depth.

#### 4.3. Comparing Depths

From the previous experiment, we found some evidence that with larger recurrent depth, the performance might improve. To further investigate various implications of depths, we carry out a systematic analysis for both recurrent depth  $d_r$  and feedforward depth  $d_f$  on *text8* and sequential MNIST datasets. We build 9 models in total with  $d_r = 1, 2, 3$  and  $d_f = 2, 3, 4$ , respectively (as shown in Figure 2(b)). We ensure that all the models have roughly the same number of parameters (e.g., the model with  $d_r = 1$  and  $d_f = 2$  has a hidden-layer size of 360).

Table 2. Test BPCs of 9 architectures with different  $d_r$ ,  $d_f$ , *tanh*

TEST BPC, <i>text8</i>	$d_r = 1$	$d_r = 2$	$d_r = 3$
$d_f = 2$	1.88	1.84	<b>1.83</b>
$d_f = 3$	1.86	1.84	1.85
$d_f = 4$	1.94	1.89	1.88

Table 2 and Figure 4 display results on the *text8* dataset. We observed that for a fixed feedforward depth  $d_f$ , increasing the recurrent depth  $d_r$  does improve the model performance, and the best test BPC is achieved by the architecture with  $d_f = 2$  and  $d_r = 3$ . This suggests that the increase of  $d_r$  can aid in better capturing the over-time nonlinearity of the input sequence. However, for a fixed  $d_r$ , increasing  $d_f$  only helps when  $d_r = 1$ . For a recurrent depth of  $d_r = 3$ , increasing  $d_f$  only hurts models performance. This can potentially be attributed to the optimization issues when modelling large input-to-output dependencies (see Appendix B.4 for more details).

With sequential MNIST dataset, we next examined the effects of  $d_f$  and  $d_r$  when modelling long term dependencies (more in Appendix B.4). In particular, we observed that increasing  $d_f$  does not bring any improvement to the model performance, and increasing  $d_r$  might even be detrimental for training. Indeed, it appears that  $d_f$  only captures the local nonlinearity and has less effect on the long term prediction. This result seems to contradict previous claims (Her-mans & Schrauwen, 2013) that stacked RNNs ( $d_f > 1$ ,

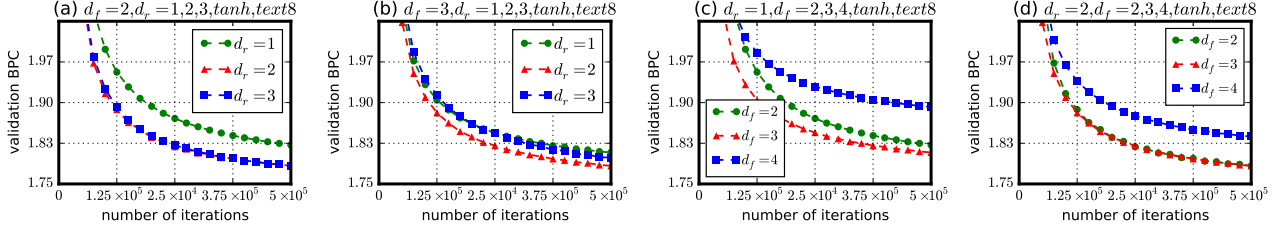


Figure 4. Validation curves for architectures with different  $d_r$  and  $d_f$ . (a) Fix  $d_f = 2$ , change  $d_r$  from 1 to 3. (b) Fix  $d_f = 3$ , change  $d_r$  from 1 to 3. (c) Fix  $d_r = 1$ , change  $d_f$  from 2 to 4. (d) Fix  $d_r = 2$ , change  $d_f$  from 2 to 4.

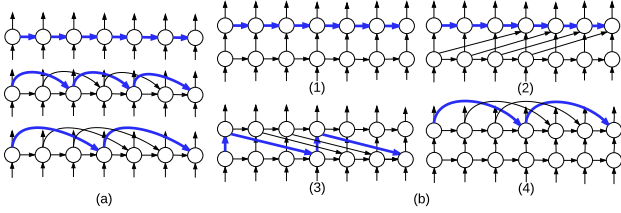


Figure 5. (a) Various architectures that we consider in Section 4.4. From top to bottom are baseline  $s = 1$ , and  $s = 2$ ,  $s = 3$ . (b) Proposed architectures that we consider in Section 4.5 where we take  $k = 3$  as an example. The shortest paths in (a) and (b) that correspond to the recurrent skip coefficients are colored in blue.

$d_r = 1$ ) could capture information in different time scales and would thus be more capable of dealing with learning long-term dependencies. On the other hand, a large  $d_r$  indicates multiple transformations per time step, resulting in greater gradient vanishing/exploding issues (Pascanu et al., 2013a), which suggests that  $d_r$  should neither be too small nor too large.

#### 4.4. Recurrent Skip Coefficients

To investigate whether increasing a recurrent skip coefficient  $s$  improves model performance on long term dependency tasks, we compare models with increasing  $s$  on the sequential MNIST problem (without/with permutation, denoted as MNIST and  $p$ MNIST).

Our baseline model is the shallow architecture proposed in Le et al. (2015). To increase the recurrent skip coefficient  $s$ , we add connections from time step  $t$  to time step  $t + k$  for some fixed integer  $k$ , shown in Figure 5 (a). By using this specific construction, the recurrent skip coefficient increases from 1 (i.e., baseline) to  $k$ . We also ensure that each model has roughly the same number of parameters: The hidden layer size of the baseline model is set to 90. Models with extra connections have 2 hidden matrices (one from  $t$  to  $t + 1$  and the other from  $t$  to  $t + k$ ), each with a size of 64.

Table 3. Test accuracies with different  $s$  for  $\tanh$  RNN

TEST ACC (%)	$s = 1$	$s = 5$	$s = 9$	$s = 13$	$s = 21$
MNIST	34.9	46.9	74.9	85.4	<b>87.8</b>
TEST ACC (%)	$s = 1$	$s = 3$	$s = 5$	$s = 7$	$s = 9$
$p$ MNIST	49.8	79.1	84.3	<b>88.9</b>	88.0

The results in Table 3 and Figure 6 show that models with recurrent skip coefficient  $s$  larger than 1 could improve the model performance dramatically. Within a reasonable range of  $s$ , test accuracy increases quickly as  $s$  becomes larger. We note that our model is the first  $\tanh$  RNN model that achieves good performance on this task, even improving upon the method proposed in Le et al. (2015).

In addition, we also formally compare with the previous results reported in Le et al. (2015); Arjovsky et al. (2015), where our model (called as sTANH) has a hidden-layer size of 95, which is about the same number of parameters as in the  $\tanh$  model of Arjovsky et al. (2015). Table 4 shows that our simple architecture improves upon the state-of-the-art by 2.6% on  $p$ MNIST, and achieves almost the same performance as LSTM on the MNIST dataset with only 25% number of parameters (Arjovsky et al., 2015).

Table 4. Test accuracies on sequential MNIST and  $p$ MNIST tasks

TEST ACC (%)	MNIST	$p$ MNIST
iRNN(LE ET AL., 2015)	97.0	$\approx 82.0$
uRNN(ARJOVSKY ET AL., 2015)	95.1	91.4
LSTM(ARJOVSKY ET AL., 2015)	<b>98.2</b>	88.0
TANH(LE ET AL., 2015)	$\approx 35.0$	$\approx 35.0$
sTANH( $s = 21, 11$ )	98.1	<b>94.0</b>

Note that obtaining good performance on sequential MNIST requires a larger  $s$  than that for  $p$ MNIST (see Appendix B.4 for more details).

#### 4.5. Recurrent Skip Coefficients vs. Skip Connections

In the next set of experiments, we investigated whether the recurrent skip coefficient can suggest something more than simply adding skip connections. We design 4 specific architectures shown in Figure 5(b): (1) is the baseline model with a 2-layer stacked architecture, the other three models add extra skip connections in different ways. Note that these extra skip connections all cross the same time length  $k$ , and in particular, (2) and (3) share quite similar architectures. However, the way in which the skip connections are allocated make a big difference on their recurrent skip coefficients: (2) has  $s = 1$ , (3) has  $s = \frac{k}{2}$  and (4) has  $s = k$ . Therefore, even though (2), (3) and (4) all add extra skip connections, the fact that their recurrent skip coefficients are different might result in different performance.

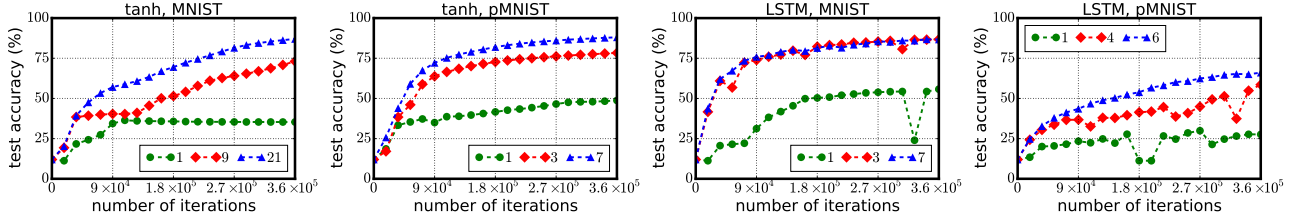


Figure 6. Test accuracies of *tanh* RNN and LSTM with different recurrent skip coefficients (numbers in the legend) on MNIST and *p*MNIST datasets.

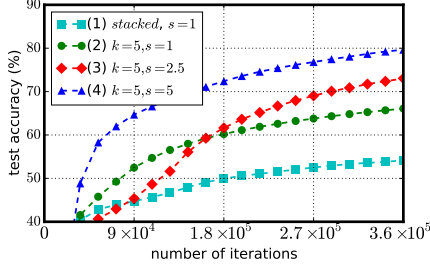


Figure 7. Test accuracy curves for architecture (1) (in cyan), (2) (in green), (3) (in red) and (4) (in blue) in Figure 5 with the  $k = 5$ .

Table 5. Test accuracies of (1), (2), (3) and (4) for *tanh* RNN

TEST ACC (%)	(1) $s = 1$	(2) $s = 1$	(3) $s = \frac{k}{2}$	(4) $s = k$
MNIST $k = 17$	39.5	39.4	54.2	<b>77.8</b>
$k = 21$	39.5	39.9	69.6	<b>71.8</b>
<i>p</i> MNIST $k = 5$	55.5	66.6	74.7	<b>81.2</b>
$k = 9$	55.5	71.1	78.6	<b>86.9</b>

We evaluated these architectures on the sequential MNIST and *p*MNIST datasets. The results show that differences in  $s$  indeed cause big performance gaps regardless of the fact that they all have skip connections (see Table 5 and Figure 7). Given the same  $k$ , the model with a larger  $s$  performs better. In particular, model (3) is better than model (2) even though they only differ in the direction of the skip connections.

It is also very interesting to see that for MNIST (unpermuted), the extra skip connection in model (2) (which does not really increase the recurrent skip coefficient) brings almost no benefits, as model (2) and model (1) have almost the same results. This observation highlights the following point: when addressing the long term dependency problems using skip connections, instead of only considering the time intervals crossed by the skip connection, one should also consider the model’s recurrent skip coefficient, which can serve as a guide for introducing more powerful skip connections.

#### 4.6. Results on LSTMs

Finally, we also performed a similar set of experiments for LSTMs. For the first experiment comparing 4 architectures

*sh*, *st*, *bu* and *td*<sup>9</sup>, as defined in Figure 2(a). LSTMs have similar performance benefits as *tanh* units, see Table 6.

Table 6. Test BPCs of *sh*, *st*, *bu*, *td* for LSTM.

TEST BPC	<i>sh</i>	<i>st</i>	<i>bu</i>	<i>td</i>
<i>text8</i>	1.65	1.66	1.65	<b>1.63</b>

LSTMs also showed performance boosts and much faster convergence speed when using larger  $s$ , as displayed in Table 7 and Figure 6. In sequential MNIST, the LSTM with  $s = 3$  already performs quite well and increasing  $s$  did not result in any significant improvement, while in *p*MNIST, the performance gradually improves as  $s$  increases from 4 to 6. We also observed that the LSTM network performed worse on permuted MNIST compared to a *tanh* RNN. Similar result was also reported in Le et al. (2015).

Table 7. Test accuracies with different  $s$  for LSTMs

TEST ACC (%)	$s = 1$	$s = 3$	$s = 5$	$s = 7$	$s = 9$
MNIST	56.2	<b>87.2</b>	86.4	86.4	84.8
TEST ACC (%)	$s = 1$	$s = 3$	$s = 4$	$s = 5$	$s = 6$
<i>p</i> MNIST	28.5	25.0	60.8	62.2	<b>65.9</b>

To conclude, the empirical evidence indicates that LSTMs might also benefit from increasing recurrent depth on some tasks and from increasing recurrent skip coefficients on long term dependency problems.

## 5. Conclusion

In this paper, we first introduced a general definition of RNNs, which allows one to construct more general architectures, and provides a solid framework for the architectural complexity analysis. We then proposed three architectural complexity measures: recurrent depth, feedforward depth, and recurrent skip coefficients, each capturing the complexity in the long term, complexity in the short term and the speed of information flow. We also find empirical evidence that increasing recurrent depth might yield performance improvements, increasing feedforward depth might

<sup>9</sup>*bu* and *td* are not well-defined within the conventional definition of an LSTM network, where a node can only receive two inputs. We overcome such limitation by considering a Multidimensional LSTM (Graves et al., 2007), which is explained in detail in Appendix B.2.



not help on long term dependency tasks, while increasing the recurrent skip coefficient can largely improve performance on long term dependency tasks. These measures and results can provide guidance for the design of new recurrent architectures for a particular learning task. Future work could involve more comprehensive studies (e.g., providing analysis on more datasets, using different architectures with various transition functions) to investigate the effectiveness of the proposed measures.

## Acknowledgments

The authors acknowledge the following agencies for funding and support: NSERC, Canada Research Chairs, CIFAR, Calcul Quebec, Compute Canada, Samsung, and IARPA Raytheon BBN Contract No. D11PC20071. The authors thank the developers of Theano (Bastien et al., 2012) and Keras (Chollet, 2015), and also thank Nicolas Ballas, Tim Cooijmans, Ryan Lowe, Mohammad Pezeshki, Roger Grosse and Alex Schwing for their insightful comments.

## References

- Arjovsky, Martin, Shah, Amar, and Bengio, Yoshua. Unitary evolution recurrent neural networks. *arXiv preprint arXiv:1511.06464*, 2015.
- Bahdanau, Dzmitry, Cho, Kyunghyun, and Bengio, Yoshua. Neural machine translation by jointly learning to align and translate. *arXiv preprint arXiv:1409.0473*, 2014.
- Bastien, Frédéric, Lamblin, Pascal, Pascanu, Razvan, Bergstra, James, Goodfellow, Ian J., Bergeron, Arnaud, Bouchard, Nicolas, and Bengio, Yoshua. Theano: new features and speed improvements. Deep Learning and Unsupervised Feature Learning NIPS 2012 Workshop, 2012.
- Bengio, Yoshua, Simard, Patrice, and Frasconi, Paolo. Learning long-term dependencies with gradient descent is difficult. *Neural Networks, IEEE Transactions on*, 5(2):157–166, 1994.
- Cho, Kyunghyun, Van Merriënboer, Bart, Gulcehre, Caglar, Bahdanau, Dzmitry, Bougares, Fethi, Schwenk, Holger, and Bengio, Yoshua. Learning phrase representations using rnn encoder-decoder for statistical machine translation. *arXiv preprint arXiv:1406.1078*, 2014.
- Chollet, François. Keras. GitHub repository: <https://github.com/fchollet/keras>, 2015.
- El Hihi, Salah and Bengio, Yoshua. Hierarchical recurrent neural networks for long-term dependencies. In *Advances in Neural Information Processing Systems*, pp. 493–499, 1996.
- Graves, Alex. Generating sequences with recurrent neural networks. *arXiv preprint arXiv:1308.0850*, 2013.
- Graves, Alex, Fernández, Santiago, and Schmidhuber, Jürgen. Multi-dimensional recurrent neural networks. In *Proceedings of the 17th International Conference on Artificial Neural Networks, ICANN’07*, pp. 549–558, Berlin, Heidelberg, 2007. Springer-Verlag. ISBN 3-540-74689-7, 978-3-540-74689-8.
- Greff, Klaus, Srivastava, Rupesh Kumar, Koutník, Jan, Steunebrink, Bas R, and Schmidhuber, Jürgen. Lstm: A search space odyssey. *arXiv preprint arXiv:1503.04069*, 2015.
- Hermans, Michiel and Schrauwen, Benjamin. Training and analysing deep recurrent neural networks. In *Advances in Neural Information Processing Systems*, pp. 190–198, 2013.
- Hochreiter, Sepp. Untersuchungen zu dynamischen neuronalen netzen. *Diploma, Technische Universität München*, 1991.
- Hochreiter, Sepp and Schmidhuber, Jürgen. Long short-term memory. *Neural computation*, 9(8):1735–1780, 1997.
- Jozefowicz, Rafal, Zaremba, Wojciech, and Sutskever, Ilya. An empirical exploration of recurrent network architectures. In *Proceedings of the 32nd International Conference on Machine Learning (ICML-15)*, pp. 2342–2350, 2015.
- Kingma, Diederik and Ba, Jimmy. Adam: A method for stochastic optimization. *arXiv preprint arXiv:1412.6980*, 2014.
- Kiros, Ryan, Zhu, Yukun, Salakhutdinov, Ruslan, Zemel, Richard S., Torralba, Antonio, Urtasun, Raquel, and Fidler, Sanja. Skip-thought vectors. In *NIPS*, 2015.
- Koutník, Jan, Greff, Klaus, Gomez, Faustino, and Schmidhuber, Jürgen. A clockwork rnn. In *Proceedings of The 31st International Conference on Machine Learning*, pp. 1863–1871, 2014.
- Le, Quoc V, Jaitly, Navdeep, and Hinton, Geoffrey E. A simple way to initialize recurrent networks of rectified linear units. *arXiv preprint arXiv:1504.00941*, 2015.
- Lin, T., Horne, B. G., Tino, P., and Giles, C. L. Learning long-term dependencies is not as difficult with NARX recurrent neural networks. *IEEE Transactions on Neural Networks*, 7(6): 1329–1338, November 1996.
- Martens, James and Sutskever, Ilya. Learning recurrent neural networks with hessian-free optimization. In *Proceedings of the 28th International Conference on Machine Learning (ICML-11)*, pp. 1033–1040, 2011.
- Mikolov, Tomáš, Sutskever, Ilya, Deoras, Anoop, Le, Hai-Son, and Kombrink, Stefan. Subword language modeling with neural networks. *preprint*, (<http://www.fit.vutbr.cz/imikolov/rnnlm/char.pdf>), 2012.
- Pascanu, Razvan, Mikolov, Tomas, and Bengio, Yoshua. Understanding the exploding gradient problem. *Computing Research Repository (CoRR) abs/1211.5063*, 2012.
- Pascanu, Razvan, Gulcehre, Caglar, Cho, Kyunghyun, and Bengio, Yoshua. How to construct deep recurrent neural networks. *arXiv preprint arXiv:1312.6026*, 2013a.
- Pascanu, Razvan, Mikolov, Tomas, and Bengio, Yoshua. On the difficulty of training recurrent neural networks. In *Proceedings of The 30th International Conference on Machine Learning*, pp. 1310–1318, 2013b.
- Raiko, Tapani, Valpola, Harri, and LeCun, Yann. Deep learning made easier by linear transformations in perceptrons. In *International Conference on Artificial Intelligence and Statistics*, pp. 924–932, 2012.

Schmidhuber, Jürgen. Learning complex, extended sequences using the principle of history compression. *Neural Computation*, 4(2):234–242, 1992.

Srivastava, Nitish, Mansimov, Elman, and Salakhutdinov, Ruslan. Unsupervised learning of video representations using LSTMs. In *ICML*, 2015.

Sutskever, Ilya and Hinton, Geoffrey. Temporal-kernel recurrent neural networks. *Neural Networks*, 23(2):239–243, 2010.

Sutskever, Ilya, Vinyals, Oriol, and Le, Quoc VV. Sequence to sequence learning with neural networks. In *Advances in neural information processing systems*, pp. 3104–3112, 2014.

---

## Supplementary Materials: Architectural Complexity Measures of Recurrent Neural Networks

---

### A. Proofs

To show theorem 3.2, we first consider the most general case in which  $d_r$  is defined (Theorem A.1). Then we discuss the mild assumptions under which we can reduce to the original limit (Proposition A.1.1). Additionally, we introduce some notations that will be used throughout the proof. If  $v = (t, p) \in \mathcal{G}_{\text{un}}$  is a node in the unfolded graph, it has a corresponding node in the folded graph, which is denoted by  $\bar{v} = (\bar{t}, p)$ .

**Theorem A.1.** *Given an RNN cyclic graph and its unfolded representation  $(\mathcal{G}_c, \mathcal{G}_{\text{un}})$ , we denote  $C(\mathcal{G}_c)$  the set of directed cycles in  $\mathcal{G}_c$ . For  $\vartheta \in C(\mathcal{G}_c)$ , denote  $l(\vartheta)$  the length of  $\vartheta$  and  $\sigma_s(\vartheta)$  the sum of  $\sigma$  along  $\vartheta$ . Write  $d_i = \limsup_{k \rightarrow \infty} \frac{\mathfrak{D}_i(n)}{n}$ .<sup>10</sup> we have :*

- The quantity  $d_i$  is periodic, in the sense that  $d_{i+m} = d_i, \forall i \in \mathbb{N}$ .
- Let  $d_r = \max_i d_i$ , then

$$d_r = \max_{\vartheta \in C(\mathcal{G}_c)} \frac{l(\vartheta)}{\sigma_s(\vartheta)} \quad (4)$$

*Proof.* The first statement is easy to prove. Because of the periodicity of the graph, any path from time step  $i$  to  $i + n$  corresponds to an isomorphic path from time step  $i + m$  to  $i + m + n$ . Passing to limit, and we can deduce the first statement.

Now we prove the second statement. Write  $\vartheta_0 = \operatorname{argmax}_{\vartheta} \frac{l(\vartheta)}{\sigma_s(\vartheta)}$ . First we prove that  $d \geq \frac{l(\vartheta_0)}{\sigma_s(\vartheta_0)}$ . Let  $c_1 = (t_1, p_1) \in \mathcal{G}_{\text{un}}$  be a node such that if we denote  $\bar{c}_1 = (\bar{t}_1, p_1)$  the image of  $c_1$  on the cyclic graph, we have  $\bar{c}_1 \in \vartheta_0$ . Consider the subsequence  $S_0 = \left\{ \frac{\mathfrak{D}_{\bar{t}_1}(k\sigma_s(\vartheta_0))}{k\sigma_s(\vartheta_0)} \right\}_{k=1}^{\infty}$  of  $\left\{ \frac{\mathfrak{D}_{\bar{t}_1}(n)}{n} \right\}_{n=1}^{\infty}$ . From the definition of  $\mathfrak{D}$  and the fact that  $\vartheta_0$  is a directed circle, we have  $\mathfrak{D}_{\bar{t}_1}(k\sigma_s(\vartheta_0)) \geq kl(\vartheta_0)$ , by considering the path on  $\mathcal{G}_{\text{un}}$  corresponding to following  $\vartheta_0$   $k$ -times. So we have

$$d_r \geq \limsup_{k \rightarrow +\infty} \frac{\mathfrak{D}_i(n)}{n} \geq \limsup_{k \rightarrow +\infty} \frac{\mathfrak{D}_{\bar{t}_1}(k\sigma_s(\vartheta_0))}{k\sigma_s(\vartheta_0)} \geq \frac{kl(\vartheta_0)}{k\sigma_s(\vartheta_0)} = \frac{l(\vartheta_0)}{\sigma_s(\vartheta_0)}$$

Next we prove  $d_r \leq \frac{l(\vartheta_0)}{\sigma_s(\vartheta_0)}$ . It suffices to prove that, for any  $\epsilon \geq 0$ , there exists  $N > 0$ , such that for any path  $\gamma : \{(t_0, p_0), (t_1, p_1), \dots, (t_{n_\gamma}, p_{n_\gamma})\}$  with  $t_{n_\gamma} - t_1 > N$ , we have  $\frac{n_\gamma}{t_{n_\gamma} - t_1} \leq \frac{l(\vartheta_0)}{\sigma_s(\vartheta_0)} + \epsilon$ . We denote  $\bar{\gamma}$  as the image of  $\gamma$  on the cyclic graph.  $\bar{\gamma}$  is a walk with repeated nodes and edges. Also, we assume there are in total  $\Gamma$  nodes in cyclic graph  $\mathcal{G}_c$ .

We first decompose  $\bar{\gamma}$  into a path and a set of directed cycles. More precisely, there is a path  $\gamma_0$  and a sequence of directed cycles  $C = C_1(\gamma), C_2(\gamma), \dots, C_w(\gamma)$  on  $\mathcal{G}_c$  such that:

- The starting and end nodes of  $\gamma_0$  is the same as  $\gamma$ . (If  $\gamma$  starts and ends at the same node, take  $\gamma_0$  as empty.)
- The catenation of the sequences of directed edges  $E(\gamma_0), E(C_1(\gamma)), E(C_2(\gamma)), \dots, E(C_w(\gamma))$  is a permutation of the sequence of edges of  $E(\gamma)$ .

The existence of such a decomposition can be proved iteratively by removing directed cycles from  $\gamma$ . Namely, if  $\gamma$  is not a paths, there must be some directed cycles  $C'$  on  $\gamma$ . Removing  $C'$  from  $\gamma$ , we can get a new walk  $\gamma'$ . Inductively apply this

---

<sup>10</sup> $\mathfrak{D}_i(n)$  is not defined when there does not exist a path from time  $i$  to time  $i + n$ . We simply omit undefined cases when we consider the limsup. In a more rigorous sense, it is the limsup of a subsequence of  $\{\mathfrak{D}_i(n)\}_{n=1}^{\infty}$ , where  $\mathfrak{D}_i(n)$  is defined.

removal, we will finally get a (possibly empty) path and a sequence of directed cycles. For a directed path or loop  $\gamma$ , we write  $D(\gamma)$  the distance between the ending node and starting node when travel through  $\gamma$  once. We have

$$D(\gamma_0) := \overline{t_{n_\gamma}} - \bar{t}_0 + \sum_{i=1}^{|\gamma_0|} \sigma(e_i)$$

where  $e_i, i \in \{1, 2, \dots, |\gamma_0|\}$  is all the edges of  $\gamma_0$ .  $\bar{t}$  denotes the module of  $t$ :  $t \equiv \bar{t} \pmod{m}$ .

So we have:

$$|D(\gamma_0)| \leq m + \Gamma \cdot \max_{e \in \mathcal{G}_c} \sigma(e) = M$$

For convenience, we denote  $l_0, l_1, \dots, l_w$  to be the length of path  $\gamma_0$  and directed cycles  $C_1(\gamma), C_2(\gamma), \dots, C_w(\gamma)$ . Obviously we have:

$$n_\gamma = \sum_{i=0}^w l_i$$

And also, we have

$$t_{n_\gamma} - t_1 = \sum_{i=1}^w \sigma_s(C_i) + D(\gamma_0)$$

So we have:

$$\frac{n_\gamma}{t_{n_\gamma} - t_1} = \frac{l_0}{t_{n_\gamma} - t_1} + \sum_{i=1}^w \frac{l_i}{t_{n_\gamma} - t_1} \leq \frac{\Gamma}{N} + \sum_{i=1}^w \frac{l_i}{t_{n_\gamma} - t_1}$$

In which we have for all  $i \in \{1, 2, \dots, w\}$ :

$$\frac{l_i}{t_{n_\gamma} - t_1} = \frac{l_i}{\sigma_s(C_i)} \cdot \frac{\sigma_s(C_i)}{t_{n_\gamma} - t_1} \leq \frac{l(\vartheta_0)}{\sigma_s(\vartheta_0)} \frac{\sigma_s(C_i)}{t_{n_\gamma} - t_1}$$

So we have:

$$\sum_{i=1}^w \frac{l_i}{t_{n_\gamma} - t_1} \leq \frac{l(\vartheta_0)}{\sigma_s(\vartheta_0)} \left[ 1 - \frac{D(\gamma_0)}{t_{n_\gamma} - t_1} \right] \leq \frac{l(\vartheta_0)}{\sigma_s(\vartheta_0)} + \frac{M'}{N}$$

in which  $M'$  and  $\Gamma$  are constants depending only on the RNN  $\mathcal{G}_c$ .

Finally we have:

$$\frac{n_\gamma}{t_{n_\gamma} - t_1} \leq \frac{l(\vartheta_0)}{\sigma_s(\vartheta_0)} + \frac{M' + \Gamma}{N}$$

take  $N > \frac{M' + \Gamma}{\epsilon}$ , we can prove the fact that  $d_r \leq \frac{l(\vartheta_0)}{\sigma_s(\vartheta_0)}$ .

□

**Proposition A.1.1.** Given an RNN and its two graph representations  $\mathcal{G}_{\text{un}}$  and  $\mathcal{G}_c$ , if  $\exists \vartheta \in C(\mathcal{G}_c)$  such that (1)  $\vartheta$  achieves the maximum in Eq.(4) and (2)  $U(\vartheta)$  in  $\mathcal{G}_{\text{un}}$  visits nodes at every time step, then we have

$$d_r = \max_{i \in \mathbb{Z}} \left( \limsup_{n \rightarrow +\infty} \frac{\mathfrak{D}_i(n)}{n} \right) = \lim_{n \rightarrow +\infty} \frac{\mathfrak{D}_i(n)}{n}$$

*Proof.* We only need to prove, in such a graph, for all  $i \in \mathbb{Z}$  we have

$$\liminf_{n \rightarrow +\infty} \frac{\mathfrak{D}_i(n)}{n} \geq \max_{i \in \mathbb{Z}} \left( \limsup_{n \rightarrow +\infty} \frac{\mathfrak{D}_i(n)}{n} \right) = d_r$$

Because it is obvious that

$$\liminf_{n \rightarrow +\infty} \frac{\mathfrak{D}_i(n)}{n} \leq d_r$$



Namely, it suffice to prove, for all  $i \in \mathbb{Z}$ , for all  $\epsilon > 0$ , there is an  $N_\epsilon > 0$ , such that when  $n > N_\epsilon$ , we have  $\frac{\mathfrak{D}_i(n)}{n} \geq d_r - \epsilon$ . On the other hand, for  $k \in \mathbb{N}$ , if we assume  $(k+1)\sigma_s(\vartheta) + i > n \geq i + k \cdot \sigma_s(\vartheta)$ , then according to condition (2) we have

$$\frac{\mathfrak{D}_i(n)}{n} \geq \frac{k \cdot l(\vartheta)}{(k+1)\sigma_s(\vartheta)} = \frac{l(\vartheta)}{\sigma_s(\vartheta)} - \frac{l(\vartheta)}{\sigma_s(\vartheta)} \frac{1}{k+1}$$

We can see that if we set  $k > \frac{\sigma_s(\vartheta)}{l(\vartheta)\epsilon}$ , the inequality we wanted to prove.

□

We now prove Proposition 3.3.1 and Theorem 3.4 as follows.

**Proposition A.1.2.** Given an RNN with recurrent depth  $d_r$ , we denote

$$d_f = \sup_{i, n \in \mathbb{Z}} \mathfrak{D}_i^*(n) - n \cdot d_r.$$

The supremum  $d_f$  exists and we have the following least upper bound:

$$\mathfrak{D}_i^*(n) \leq n \cdot d_r + d_f.$$

*Proof.* We first prove that  $d_f < +\infty$ . Write  $d_f(i) = \sup_{n \in \mathbb{Z}} \mathfrak{D}_i^*(n) - n \cdot d_r$ . It is easy to verify  $d_f(\cdot)$  is  $m$ -periodic, so it suffices to prove for each  $i \in \mathbb{N}$ ,  $d_f(i) < +\infty$ . Hence it suffices to prove

$$\limsup_{n \rightarrow \infty} (\mathfrak{D}_i^*(n) - n \cdot d_r) < +\infty.$$

From the definition, we have  $\mathfrak{D}_i(n) \geq \mathfrak{D}_i^*(n)$ . So we have

$$\mathfrak{D}_i^*(n) - n \cdot d_r \leq \mathfrak{D}_i(n) - n \cdot d_r.$$

From the proof of Theorem A.1, there exists two constants  $M'$  and  $\Gamma$  depending only on the RNN  $\mathcal{G}_c$ , such that

$$\frac{\mathfrak{D}_i(n)}{n} \leq d_r + \frac{M' + \Gamma}{n}.$$

So we have

$$\limsup_{n \rightarrow \infty} (\mathfrak{D}_i^*(n) - n \cdot d_r) \leq \limsup_{n \rightarrow \infty} (\mathfrak{D}_i(n) - n \cdot d_r) \leq M' + \Gamma.$$

Also, we have  $d_f = \sup_{i, n \in \mathbb{Z}} \mathfrak{D}_i^*(n) - n \cdot d_r$ , so for any  $i, n \in \mathbb{Z}$ ,

$$d_f \geq \mathfrak{D}_i^*(n) - n \cdot d_r.$$

□

**Theorem A.2.** Given an RNN and its two graph representations  $\mathcal{G}_{\text{un}}$  and  $\mathcal{G}_c$ , we denote  $\xi(\mathcal{G}_c)$  the set of directed path that starts at an input node and ends at an output node in  $\mathcal{G}_c$ . For  $\gamma \in \xi(\mathcal{G}_c)$ , denote  $l(\gamma)$  the length and  $\sigma_s(\gamma)$  the sum of  $\sigma$  along  $\gamma$ . Then we have:

$$d_f = \sup_{i, n \in \mathbb{Z}} \mathfrak{D}_i^*(n) - n \cdot d_r = \max_{\gamma \in \xi(\mathcal{G}_c)} l(\gamma) - \sigma_s(\gamma) \cdot d_r.$$

*Proof.* Let  $\gamma : \{(t_0, 0), (t_1, p_1), \dots, (t_{n_\gamma}, p)\}$  be a path in  $\mathcal{G}_{\text{un}}$  from an input node  $(t_0, 0)$  to an output node  $(t_{n_\gamma}, p)$ , where  $t_0 = i$  and  $t_{n_\gamma} = i + n$ . We denote  $\bar{\gamma}$  as the image of  $\gamma$  on the cyclic graph. From the proof of Theorem A.1, for each  $\bar{\gamma}$  in  $\mathcal{G}_c$ , we can decompose it into a path  $\gamma_0$  and a sequence of directed cycles  $C = C_1(\gamma), C_2(\gamma), \dots, C_w(\gamma)$  on  $\mathcal{G}_c$  satisfying those properties listed in Theorem A.1. We denote  $l_0, l_1, \dots, l_w$  to be the length of path  $\gamma_0$  and directed cycles  $C_1(\gamma), C_2(\gamma), \dots, C_w(\gamma)$ . We know  $\frac{l_k}{\sigma_s(C_k)} \leq d_r$  for all  $k = 1, 2, \dots, w$  by definition. Thus,

$$\begin{aligned} l_k &\leq d_r \cdot \sigma_s(C_k) \\ \sum_{k=1}^w l_k &\leq d_r \cdot \sum_{k=1}^w \sigma_s(C_k) \end{aligned}$$

Note that  $n = \sigma_s(\gamma_0) + \sum_{k=1}^w \sigma_s(C_k)$ . Therefore,

$$\begin{aligned} l(\gamma) - n \cdot d_r &= l_0 + \sum_{k=1}^w l_k - n \cdot d_r \\ &\leq l_0 + d_r \cdot \left( \sum_{k=1}^w \sigma_s(C_k) - n \right) \\ &= l_0 - d_r \cdot \sigma_s(\gamma_0) \end{aligned}$$

for all time step  $i$  and all integer  $n$ . The above inequality suggests that in order to take the supremum over all paths in  $\mathcal{G}_{\text{un}}$ , it suffices to take the maximum over a directed path in  $\mathcal{G}_c$ . On the other hand, the equality can be achieved simply by choosing the corresponding path of  $\gamma_0$  in  $\mathcal{G}_{\text{un}}$ . The desired conclusion then follows immediately.  $\square$

Lastly, we show Theorem 3.6.

**Theorem A.3.** *Given an RNN cyclic graph and its unfolded representation  $(\mathcal{G}_c, \mathcal{G}_{\text{un}})$ , we denote  $C(\mathcal{G}_c)$  the set of directed cycles in  $\mathcal{G}_c$ . For  $\vartheta \in C(\mathcal{G}_c)$ , denote  $l(\vartheta)$  the length of  $\vartheta$  and  $\sigma_s(\vartheta)$  the sum of  $\sigma$  along  $\vartheta$ . Write  $s_i = \liminf_{k \rightarrow \infty} \frac{\mathfrak{d}_i(n)}{n}$ . We have :*

- The quantity  $s_i$  is periodic, in the sense that  $s_{i+m} = s_i, \forall i \in \mathbb{N}$ .
- Let  $s = \min_i s_i$ , then

$$d_r = \min_{\vartheta \in C(\mathcal{G}_c)} \frac{l(\vartheta)}{\sigma_s(\vartheta)}. \quad (5)$$

*Proof.* The proof is essentially the same as the proof of the first theorem. So we omit it here.  $\square$

**Proposition A.3.1.** *Given an RNN and its two graph representations  $\mathcal{G}_{\text{un}}$  and  $\mathcal{G}_c$ , if  $\exists \vartheta \in C(\mathcal{G}_c)$  such that (1)  $\vartheta$  achieves the minimum in Eq.(5) and (2)  $U(\vartheta)$  in  $\mathcal{G}_{\text{un}}$  visits nodes at every time step, then we have*

$$s = \min_{i \in \mathbb{Z}} \left( \liminf_{n \rightarrow +\infty} \frac{\mathfrak{d}_i(n)}{n} \right) = \lim_{n \rightarrow +\infty} \frac{\mathfrak{d}_i(n)}{n}.$$

*Proof.* The proof is essentially the same as the proof of the Proposition A.1.1. So we omit it here.  $\square$

## B. Experiment Details

### B.1. RNNs with $\tanh$

In this section we explain the functional dependency among nodes in RNNs with  $\tanh$  in detail.

The transition function for each node is the  $\tanh$  function. The output of a node  $v$  is a vector  $h_v$ . To compute the output for an node, we simply take all incoming nodes as input, and sum over their affine transformations and then apply the  $\tanh$  function (we omit the bias term for simplicity).

$$h_v = \tanh \left( \sum_{u \in \text{In}(v)} \mathbf{W}(u) h_u \right),$$

where  $\mathbf{W}(\cdot)$  represents a real matrix.

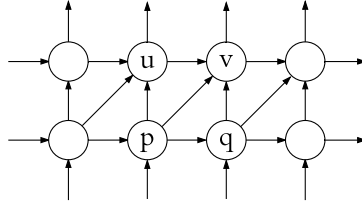


Figure 8. “Bottom-up” architecture (*bu*).

As a more concrete example, consider the “bottom-up” architecture in Figure 8, with which we did the experiment described in Section 4.2. To compute the output of node  $v$ ,

$$h_v = \tanh(\mathbf{W}(u)h_u + \mathbf{W}(p)h_p + \mathbf{W}(q)h_q). \quad (6)$$

### B.2. LSTMs

In this section we explain the Multidimensional LSTM (introduced by (?)) which we use for experiments with LSTMs (see Section 4.6).

The output of a node  $v$  of the LSTM is a 2-tuple  $(c_v, h_v)$ , consisting of a cell memory state  $c_v$  and a hidden state  $h_v$ . The transition function  $F$  is applied to each node indistinguishably. We describe the computation of  $F$  below in a sequential manner (we omit the bias term for simplicity).

$$\begin{aligned} z &= g \left( \sum_{u \in \text{In}(v)} \mathbf{W}_z(u) h_u \right) && \text{block input} \\ i &= \sigma \left( \sum_{u \in \text{In}(v)} \mathbf{W}_i(u) h_u \right) && \text{input gate} \\ o &= \sigma \left( \sum_{u \in \text{In}(v)} \mathbf{W}_o(u) h_u \right) && \text{output gate} \\ \{f_u\} &= \left\{ \sigma \left( \sum_{u' \in \text{In}(v)} \mathbf{W}_{f_u}(u') h_{u'} \right) \mid u \in \text{In}(v) \right\} && \text{A set of forget gates} \\ c_v &= i \odot z + \sum_{u \in \text{In}(v)} f_u \odot c_u && \text{cell state} \\ h_v &= o \odot c_v && \text{hidden state} \end{aligned}$$

Note that the Multidimensional LSTM includes the usual definition of LSTM as a special case, where the extra forget gates are 0 (i.e., bias term set to  $-\infty$ ) and extra weight matrices are 0. We again consider the architecture *bu* in Fig. 8. We first

compute the block input, the input gate and the output gate by summing over all affine transformed outputs of  $u, p, q$ , and then apply the activation function. For example, to compute the input gate, we have

$$i = \sigma(\mathbf{W}_i(u)h_u + \mathbf{W}_i(p)h_p + \mathbf{W}_i(q)h_q).$$

Next, we compute one forget gate for each pair of  $(v, u), (v, p), (v, q)$ . The way of computing a forget gate is the same as computing the other gates. For example, the forget gate in charge of the connection of  $u \rightarrow v$  is computed as,

$$f_u = \sigma(\mathbf{W}_{f_u}(u)h_u + \mathbf{W}_{f_u}(p)h_p + \mathbf{W}_{f_u}(q)h_q).$$

Then, the cell state is simply the sum of all element-wise products of the input gate with the block output and forget gates with the incoming nodes' cell memory states,

$$c_v = i \odot z + f_u \odot c_u + f_p \odot c_p + f_q \odot c_q.$$

Lastly, the hidden state is computed as usual,

$$h_v = o \odot c_v.$$

### B.3. Recurrent Depth is Non-trivial

The validation curves of the 4 different connecting architectures  $sh, st, bu$  and  $td$  on text8 dataset for both  $\tanh$  and LSTM are shown below:

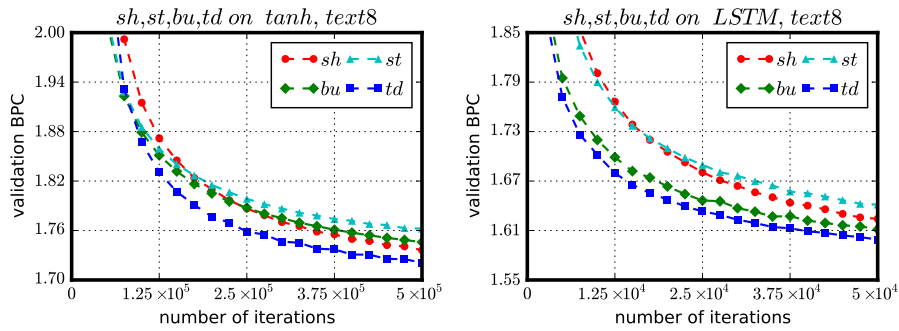


Figure 9. Validation curves for  $sh, st, bu$  and  $td$  on test8 dataset. Left: results for  $\tanh$ . Right: results for LSTM.

### B.4. Full Comparisons on Depths

Figure 10 and Figure 11 show all the validation curves for the 9 architectures on text8 dataset, with their  $d_r = 1, 2, 3$  and  $d_f = 2, 3, 4$  respectively. We use two initialization schemes: In Figure 10, hidden-to-hidden matrices are initialized from uniform distribution, while in Figure 11, hidden-to-hidden matrices are initialized using orthogonal matrices. In Figure 11, we observe that orthogonal initialization helps for the optimization issues when  $d_f$  is large, in which increasing  $d_f$  does not harm the learning. While the results are still consistent with our analysis in the main paper. Notice that one can achieve better results with much larger models on this dataset, as in (?).

Also, to see if increasing feedforward depth/ recurrent depth helps for long term dependency problems, we evaluate these 9 architectures on sequential MNIST task, with roughly the same number of parameters( 8K, where the first architecture with  $d_r = 1$  and  $d_f = 2$  has hidden size of 90.). We try two initialization schemes where hidden-to-hidden matrices are initialized from uniform distribution or using orthogonal matrices.

Figure 12 and 13 clearly show that, as the feedforward depth increases, the model performance stays roughly the same. In addition, note that increasing recurrent depth might even result in performance decrease. This is possibly because that larger recurrent depth amplifies the gradient vanishing/exploding problems, which is detrimental on long term dependency tasks.



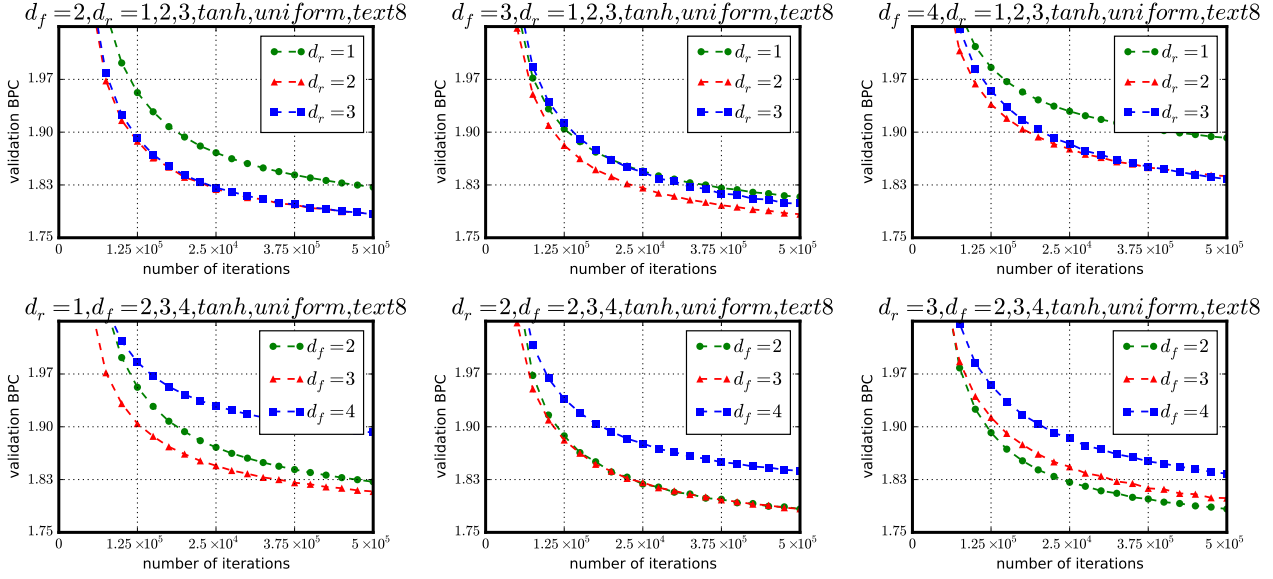


Figure 10. Validation curves of 9 architectures with feedforward depth  $d_f = 2, 3, 4$  and recurrent depth  $d_r = 1, 2, 3$  on test8 dataset. **Hidden-to-hidden matrices are initialized from uniform distribution.** For each figure in the first row, we fix  $d_r$  and draw 3 curves with different  $d_f = 2, 3, 4$ . For each figure in the second row, we fix  $d_f$  and draw 3 curves with different  $d_r = 2, 3, 4$ .

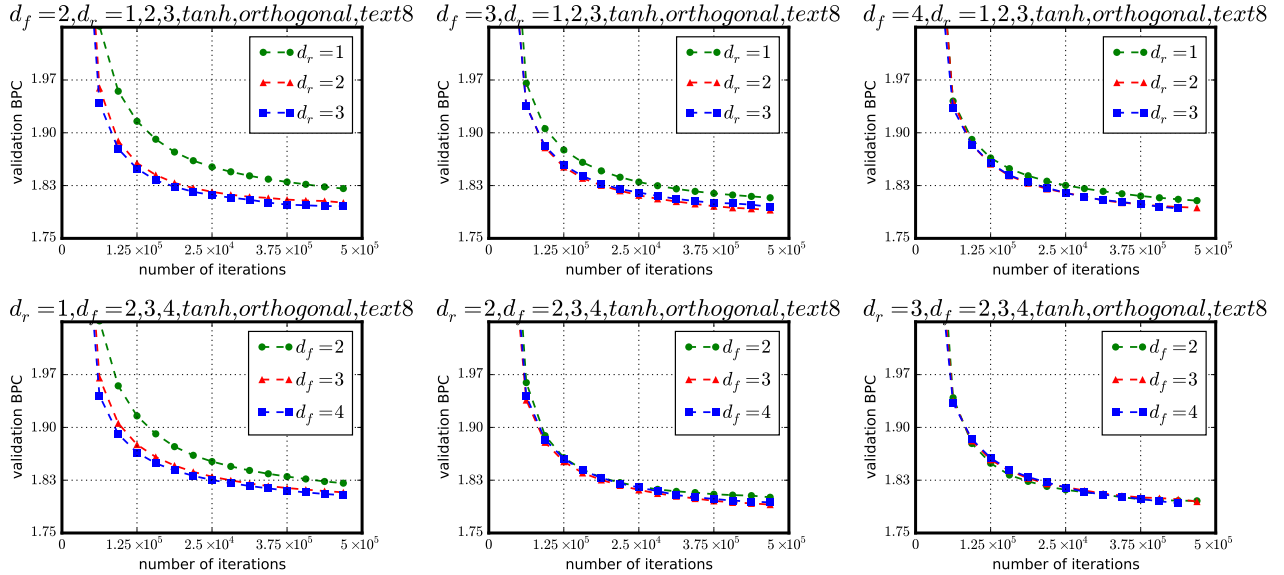


Figure 11. Validation curves of 9 architectures with feedforward depth  $d_f = 2, 3, 4$  and recurrent depth  $d_r = 1, 2, 3$  on test8 dataset. **Hidden-to-hidden matrices are initialized using orthogonal matrices.** For each figure in the first row, we fix  $d_r$  and draw 3 curves with different  $d_f = 2, 3, 4$ . For each figure in the second row, we fix  $d_f$  and draw 3 curves with different  $d_r = 2, 3, 4$ .

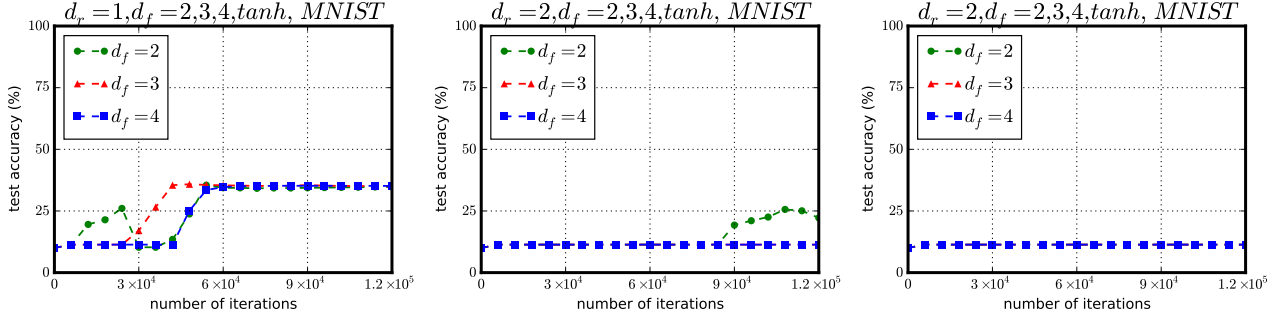


Figure 12. Test accuracies of 9 architectures with feedforward depth  $d_f = 2, 3, 4$  and recurrent depth  $d_r = 1, 2, 3$  on sequential MNIST. For each figure, we fix  $d_r$  and draw 3 curves with different  $d_f$ . **Hidden-to-hidden matrices are initialized from uniform distribution.**

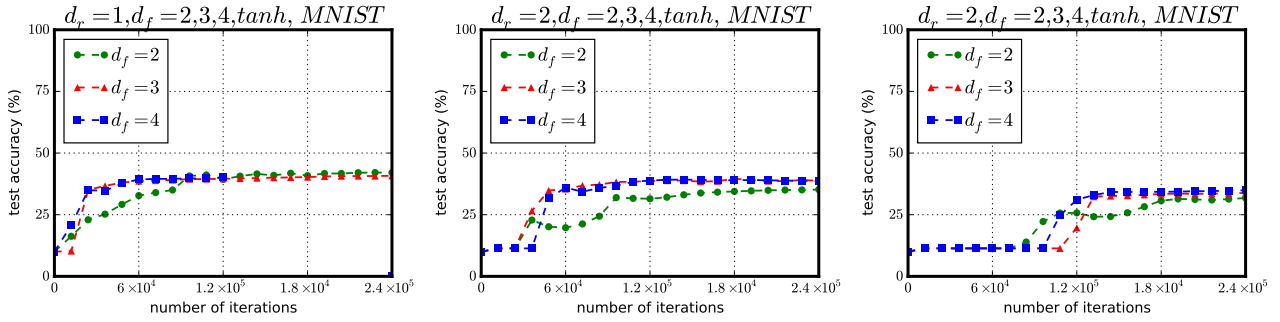


Figure 13. Test accuracies of 9 architectures with feedforward depth  $d_f = 2, 3, 4$  and recurrent depth  $d_r = 1, 2, 3$  on sequential MNIST. For each figure, we fix  $d_r$  and draw 3 curves with different  $d_f$ . **Hidden-to-hidden matrices are initialized using orthogonal matrices.**

### B.5. Recurrent Skip Coefficients

The test curves for all the experiments are shown in Figure 14. In Figure 14, we observed that obtaining good performance on MNIST requires larger  $s$  than for pMNIST. We hypothesize that this is because, for the sequential MNIST dataset, each training example contains many consecutive zero-valued subsequences, each of length 10 to 20. Thus within those subsequences, the input-output gradient flow could tend to vanish. However, when the recurrent skip coefficient is large enough to cover those zero-valued subsequences, the model starts to perform better. With pMNIST, even though the random permuted order seems harder to learn, the permutation on the other hand blends zeros and ones to form more uniform sequences, and this may explain why training is easier, less hampered by the long sequences of zeros.

### B.6. Recurrent Skip Coefficients vs. Skip Connections

Test curves for all the experiments are shown in Figure 15. Observe that in most cases, the test accuracy of (3) is worse than (2) in the beginning while beating (2) in the middle of the training. This is possibly because in the first several time steps, it is easier for (2) to pass information to the output thanks to the skip connections, while only after multiples of  $k$  time steps, (3) starts to show its advantage with recurrent skip connections<sup>11</sup>. The shorter paths in (2) make its gradient flow more easily in the beginning, but in the long run, (3) seems to be more superior, maybe because of its more prominent skipping effect over time.

<sup>11</sup>It will be more clear if one checks the length of the shortest path from a node at time  $t$  to a node at time  $t+k$  in both architectures.

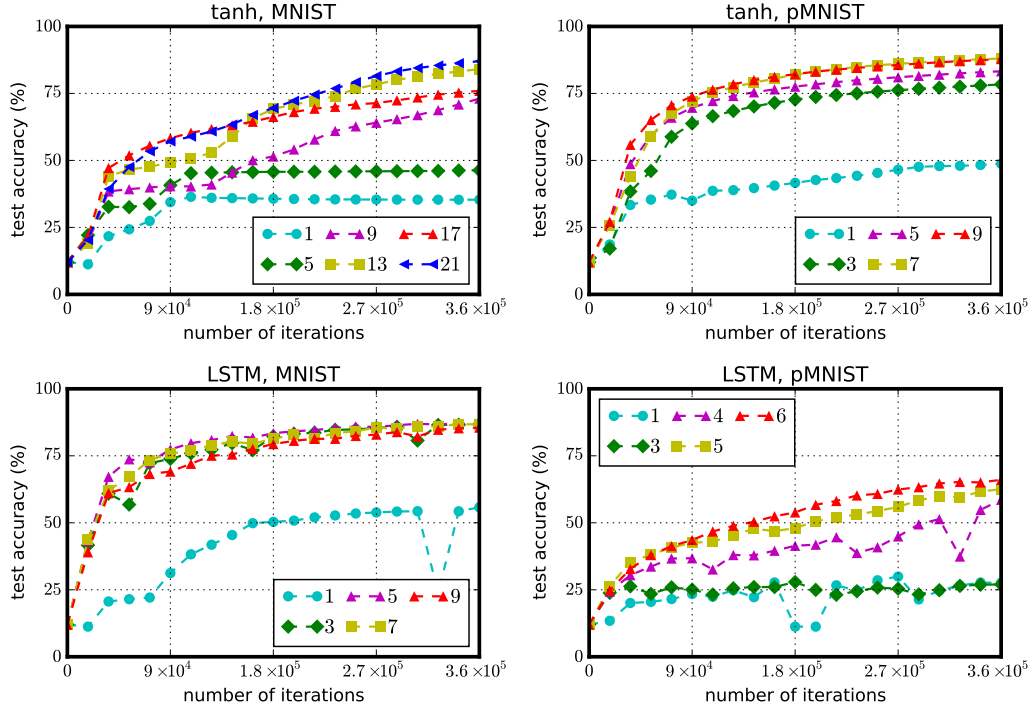


Figure 14. Test curves on MNIST/pMNIST, with *tanh* and *LSTM*. The numbers in the legend denote the recurrent skip coefficient  $s$  of each architecture.

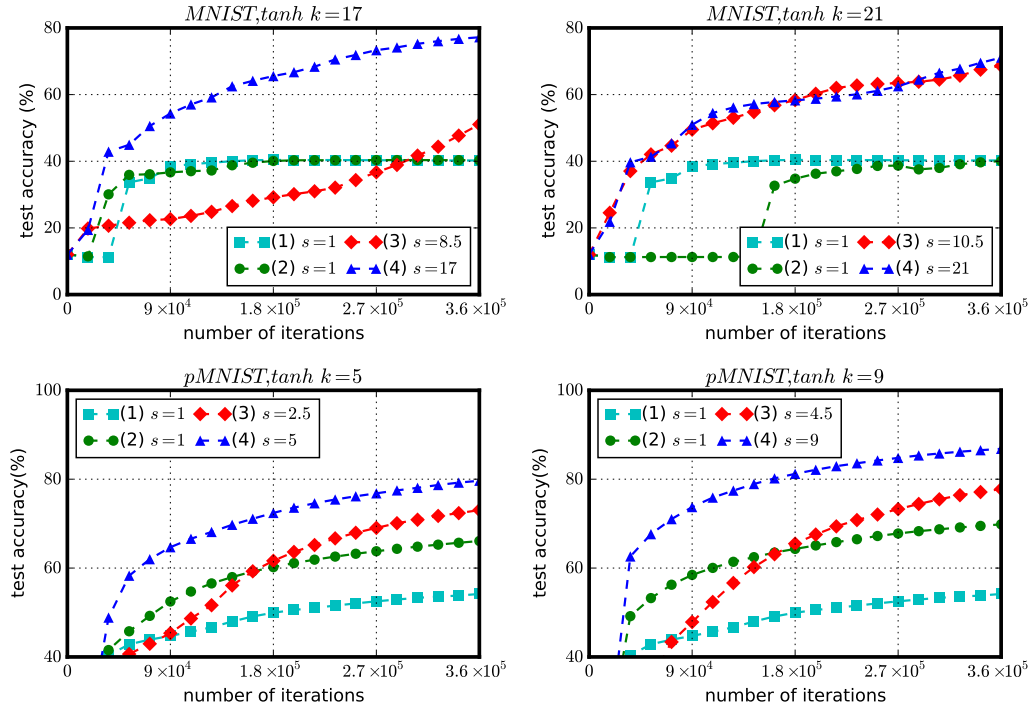


Figure 15. Test curves on MNIST/pMNIST for architecture (1), (2), (3) and (4), with *tanh*. The recurrent skip coefficient  $s$  of each architecture is shown in the legend.